SUPPORTING MATERIAL

Functional importance of short range binding and long range solvent interactions in helical anti-freeze peptides

Simon Ebbinghaus, Konrad Meister, Maxim B. Prigozhin, Arthur L. DeVries, Martina Havenith, Joachim Dzubiella, and Martin Gruebele

[†]Department of Physical Chemistry II, Ruhr-Universität Bochum, D-44780 Bochum, Germany
Departments of [‡]Chemistry, [&]Animal Biology, [¶]Physics, and Center for Biophysics and Computational Biology, University of Illinois, Urbana, Illinois, USA 61801
[#]Department of Physics, Humboldt University of Berlin, 12489 Berlin, and Helmholtz-Zentrum Berlin für Materialien und Energie GmbH, 14109 Berlin, Germany

Mutant choice and secondary structure stability

Mutation sites were chosen based on the review by Harding *et al.* (reference 6 in the main text). To measure overall helix rigidity by FRET, we needed a chromophore near one of the termini. A33E and A33Q mutations were reported to have little effect on antifreeze activity, so we chose the A33W substitution. Hysteresis and CD measurements confirmed high activity (main text Figure 1) and large helix content at low temperature at least (see Figure S2 below). The SASW, TLTW and VAVW were also chosen based on Harding *et al*. They found that SASA and TLTA had zero activity, while VAVA had 85% activity at 2 mM peptide concentration. Our VAVA measurements show only 30% activity at 2 mM , but activity climbs slowly to 60% at high concentrations (> 10 mM). The discrepancy could be due to buffer conditions. (Our hysteresis and CD experiments were carried out in 100 mM ammonium biphosphate.) Despite these differences, the VAVW mutant clearly retain more activity than TLTW and SASW, the tryptophan analogs of the mutants studied by Harding *et al.*, so we agree with their activity ranking qualitatively.

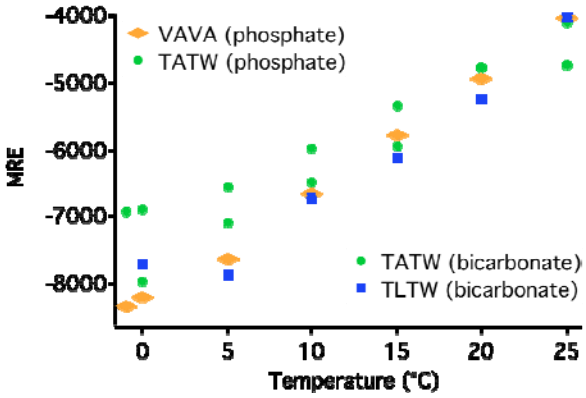

FIGURE S1 CD melting curve of the pseudo-wildtype TATW, its mutant TLTW (A17L), and VAVA, which was previously studied by Harding *et al*. (see reference in main text). At low temperature, they approach the same mean residue ellipticity as the WT protein (see Figure 2 in main text).

Although TATW, TLTW, VAVW and the non-tryptophan mutant VAVA have only half the helix content of the TATA wild type at room temperature (as assessed by the 208 and 222 nm peaks in their CD spectra), they gain considerable secondary structure at lower temperature. As shown in Figure S1 below, their thermal melts are very similar. The overall secondary structure content is only minimally disrupted by the additional A17L mutation of TLTW compared to TATV, although TLTW preferentially forms a two-helix bundle in MD simulations. VAVA, previously studied by Harding *et al*., gains slightly more structure at low temperature than TATW in phosphate buffer. The ammonium bicarbonate buffer promotes most helix formation at low temperature in the TATW tryptophan mutant that is our pseudo-wild type.

Hysteresis measurements and buffer dependence

Freezing and melting points were determined with a Clifton Nanoliter Cryoscope (Clifton, New Jersey). The cryoscope utilizes a temperature controlled Peltier sample holder that fits on a microscope stage and the sample holder temperature varies only ±0.01°C about the set point. Six 600 μm diameter wells were loaded with heavy microscope immersion oil (Type B) and 3 to 5 nanoliter of the aqueous antifreeze solution was inserted into the center of each oil-filled well with a micropipette. The magnification was 200 times.

The samples were cooled to -30 to -40 °C, and the frozen sample slowly warmed until only a single disc shaped ice crystal remained (10-15 μm diameter). The melting point of this seed crystal was equated to the equilibrium freezing point. Upon slowly cooling the single small ice crystal at 0.05 °C per minute, it grew into a blunt hexagonal bipyramid (HBP) at 0.05 °C below the melting point. For the wild type and the active mutants TATW and VAVW, no additional growth was observed during cooling until complete freezing occurred. The wild type growth at the freezing point was in the form of C-axis needles propagating from the tip of the HBP, which upon reaching the edge of the aqueous sphere began to increase in diameter.

In the case of the active mutants the HBP that formed slightly below the melting point varied in morphology: the most active TATW grew into a HBP with an axial ratio of 1:4-5, while VAVW formed a truncated HBP. In contrast to the wild type there was an equal expansion and elongation of the HBP at the freezing point with these two mutants. At low concentrations of VAVA, slow growth occurred in the hysteresis gap near the melting point in the form of extension and expansion of the HBP. With inactive mutants SASW and TLTW, growth began immediately slightly below the melting point in the form of irregular hexagons which enlarged and thickened until the entire aqueous sphere was solid.

As seen in the previous section, secondary structure is somewhat buffer-dependent. In the main text, hysteresis activity is shown in ammonium bicarbonate buffer, which promoted the solubility of some of the less soluble peptides (e.g. VAVA and VAVW). Figure S2 compares the hysteresis of our pseudo-wild type TATW and VAVA. The ordering of activity is preserved, but both are less active in pure water than in 100 mM ammonium bicarbonate buffer. Li et al. (reference 7 in the main text) showed that small solutes such as ammonium sulfate or bicarbonate enhance insect antifreeze protein activity, and such enhancements also occur for the fish proteins. The proteins evolved to function at non-zero ionic strength in fish, so it is not surprising that they might be less

active in pure water. The data in the main text and in Figure S2 were fitted to the Langmuir-Hill equation, which describes chemical adsorption reaction (here AFPs absorbing to ice surfaces slightly below the water freezing point):

$$y(c) = \frac{A(c/c50)^r}{1+(c/c50)^r}$$

where A is the maximum coverage, $c50$ the concentration of half coverage, and r a cooperativity exponent (r=1 in the Langmuir equation, r can differ from 1 in the Hill equation).

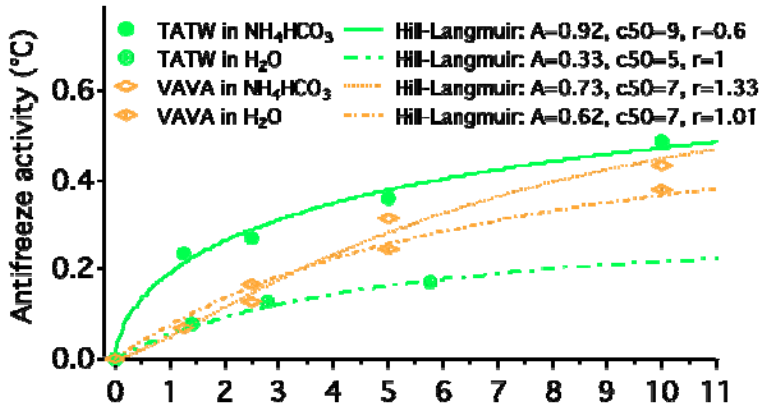

FIGURE S2 Hysteresis of the pseudo-WT TATW, and the mutant VAVA, previously studied by Harding *et al*. Activity in water is reduced compared to water solvent, as evidenced by lower asymptotic values in the Langmuir-Hill equation.

FRET measurement and modeling

The absence of aggregation during FRET measurements was checked by spinning down samples, diluting by a factor of 3 and re-measuring FRET. Similar results were obtained with the less concentrated samples. To compute integrated intensities, Raman scatter and grating bleed-through (second order diffraction peaks) were subtracted yielding a ±3% error in FRET detection. FRET labeling did not have a significant effect on CD spectra where comparison was made.

We developed a code based on the LabView programming language to calculate FRET efficiencies E by statistically sampling distances R between the donor (W33) and the acceptor (N-terminal Dansyl moiety):

$$E = \frac{1}{1+(R/R_0)^6}$$

We modeled two extreme cases: a completely stiff helix, and two stiff helical segments connected by a flexible linker. For each calculation 100000 micro-states with different values of R were sampled. An R_o value of 2.1 nm was used in each case. E was calculated for each value of R and averaged over all micro-states.

1) The rigid helix was modeled as a segment of 4.8 nm length from the N-terminus to the center of the Trp 33 sidechain (average distance based on the TATW MD simulation, see

below). The center of the Dansyl group was modeled as a completely flexible segment of length 0.5 nm attached to the N-terminus, and was sampled to have full angular flexibility (such that the complete set of allowed conformations would form a sphere with the N-terminus at its center). The average over 100000 values of R yielded E_{FRET} = 1%.

2) To model a kinked helix, we used the time series from MD simulation (see below) as an input for the Dansyl-W33 FRET pair distance R. The distances were sampled at random from the TLTW MD trajectory at t>70 ns. In this case we obtained E_{FRET} = 37%.

MD simulation

The continuous MD simulations were performed using the simulation package AMBER9.0 with the ff03 force field (reference 8 in the main text) and the SPC/E water model (reference 9 in the main text) in the constant number (N), pressure (P), and temperature (T) ensemble. The proteins were solvated by ~6000 water molecules with fully α-helical initial backbone configurations (taken from the crystal structure) in periodically repeated truncated octahedron boxes. The pressure was maintained at P =1 bar by a weak-coupling barostat and the temperature T = 274 kept constant by a Langevin thermostat. The long-ranged electrostatics was handled by particle-mesh Ewald summation using AMBER default parameters. Short-ranged electrostatics and dispersion interactions were cut-off at 0.9 nm. Trajectory data was written every 10 ps. Five peptides were simulated, the wildtype TATA and four with the A33W background mutation, TATW, TLTW, SASW, and VAVW as described in the main text. All were initially simulated for over 30 ns, the TATW and TLTW runs were continued to ~170 ns. Trajectory analysis was done using the *ptraj* tool in the Amber package, where, in particular, secondary structure elements (SSE) such as the α-helicity (i.e., helix percentage per peptide configuration) are identified using the DSSP method by Kabsch and Sander (reference 10 in the main text). As described in the main text after ~70 ns a major structural transition into the kinked state was found for the TLTW double mutant with the kink being at position 16 adjacent to the mutation, while the total average helicity remained nearly unchanged at 80-90%. The novel structure in TLTW was identfied as a kinked configuration with two a-helical segments and the kink being exactly adjacent to the position of the mutation TLTW, as shown in the representative snapshot in Figure 3b of the main text). Note that two of the Thr-Thr spacings remain intact, while the middle one is disrupted (Figure S3ab structures, dark blue side chains)

For equilibrium sampling of possible conformational changes, we performed replica exchange MD (REMD) simulations for all 5 proteins using initial configurations from the simulations described above. In total 48 replicas were simulated per protein with temperatures T = 280.00, 282.32, 284.66, 287.01, 289.38, 291.77, 294.17, 296.58, 299.02, 301.46, 303.92, 306.40, 308.90, 311.41, 313.94, 316.48, 319.04, 321.63, 324.22, 326.83, 329.46, 332.11, 334.78, 337.46, 340.16, 342.88, 345.61, 348.37, 351.14, 353.93, 356.74, 359.57, 362.41, 365.28, 368.16, 371.06, 373.99, 376.93, 379.89, 382.88, 385.88, 388.90, 391.94, 395.00, 398.08, 401.19, 404.31, 407.45 K. Every replica was simulated for 65-85 ns. Replica exchanges were attempted every 250 integration steps. We plot the average SSE resolved by residue number in Figure S3 for all proteins ns for T=280 K for at least the last 60 ns. Judging from the evolution of SSE in time, it seems that within the last 30 ns the SSE distribution does not change significantly as we have reached

equilibrium. Here, the REMD simulations confirm local weaknesses of the helical state for all peptides sensitive to point mutations. The α-helical structure of the TLTW double and SASW triple mutants is locally slightly less stable than WT and TATW pseudo-WT with respect to thermal fluctuations adjacent to the position of the mutation A17L, and this was sufficient to induce a kinked state in the brute-force simulation. The analysis of secondary structure reveals structural fluctuations and overall destabilization around the mutation site of TLTW and particularly VAVW, which undergoes transitions to coil over several residues twice during the simulation (white areas in Figure S3d), whereas the effect is much less pronounced for the SASW mutant. Thus, both single trajectory and REMD molecular dynamics simulations strongly point to an extended-kinked equilibrium of TLTW, frequent helix-to-coil transitions of VAVW, and a more stable helical structure for SASW.

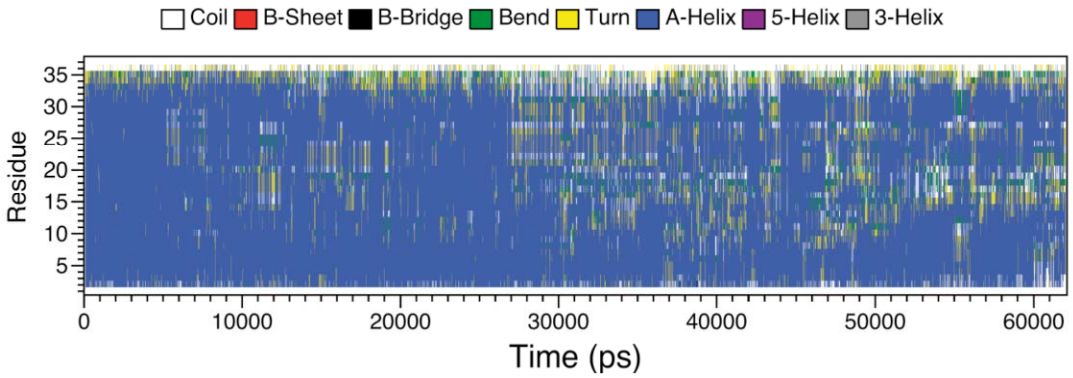

FIGURE S3a TATA (wild type) secondary structure elements.

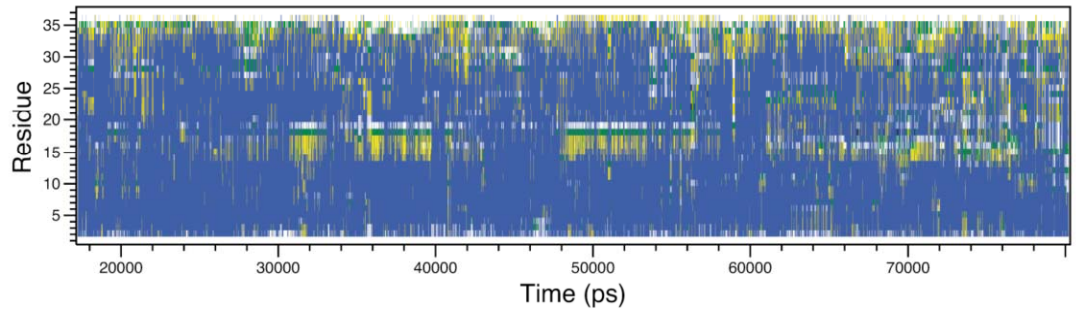

FIGURE S3b TATW mutant secondary structure elements.

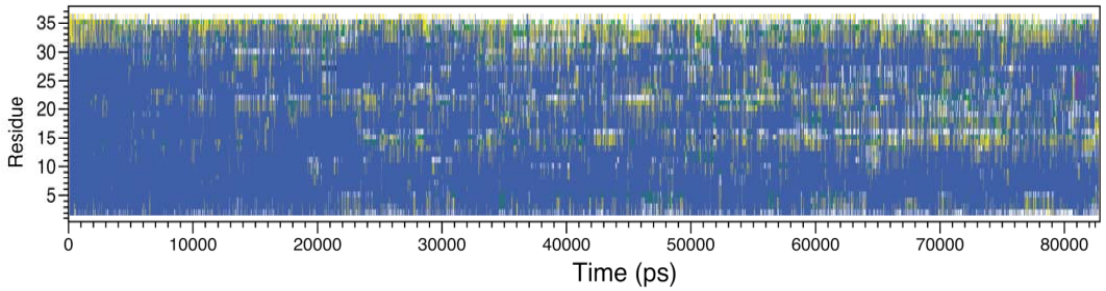

FIGURE S3c SASW mutant secondary structure elements.

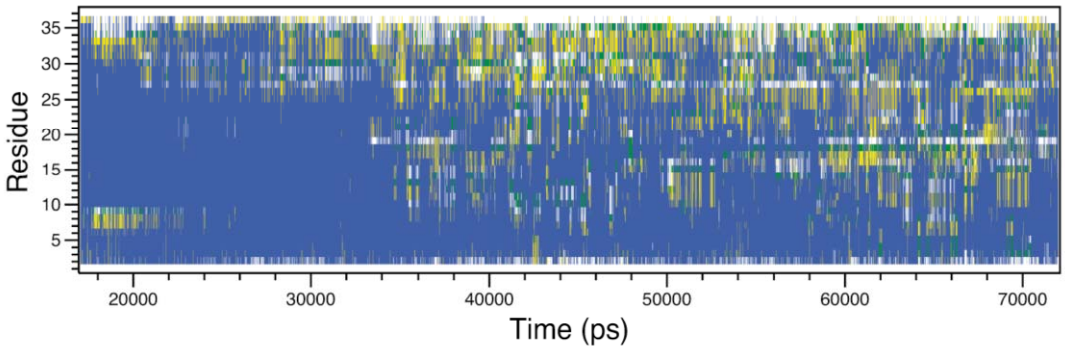

FIGURE S3d TLTW mutant secondary structure elements.

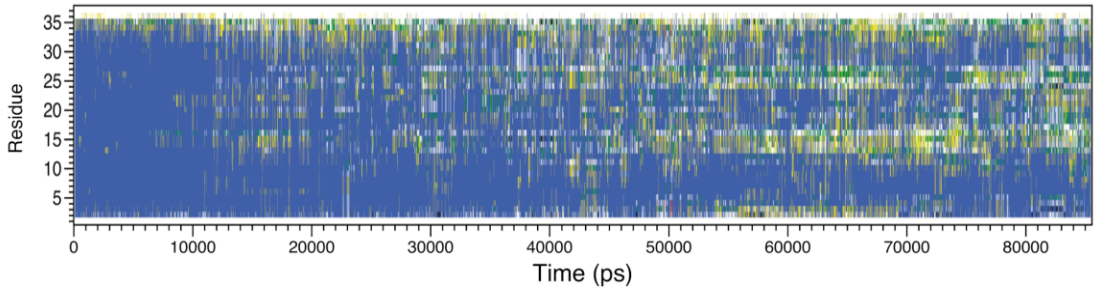

FIGURE S3e VAVW mutant secondary structure elements.

Figure S3. All parts of the Figure show Replica Exchange Molecular Dynamics Simulations (REMD) analyzing the secondary structure of wf-AFP1 mutants. Simulations sample 48 replicas with at least 65 ns per replica for the temperature range from 280 to 410 K. Shown are at least the last 50 ns of the runs for *T* = 280 K.